Fuel 422 (2026) 139124

Contents lists available at ScienceDirect

Fuel

journal homepage: www.elsevier.com/locate/fuel

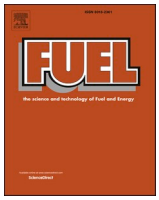

Full Length Article

Modelling hydrogen enriched ammonia combustion through laminar flame speed and mass fraction burn analysis

D.N. Rrustemi *, T. Megaritis, L.C. Ganippa

Department of Mechanical and Aerospace Engineering, Brunel University of London, Uxbridge, London UB8 3PH, UK

ARTICLE INFO

Keywords:
Ammonia
Dual fuel
Exhaust gas recirculation
Hydrogen
Two-zone model

ABSTRACT

Ammonia is a promising zero-carbon fuel for internal combustion engines; however, its low laminar flame speed makes lean combustion highly sensitive to turbulence and flame development. In this study, an entrainment-based two-zone combustion model is developed for hydrogen-enriched ammonia spark-ignition engines. The novelty of the approach lies in calibrating turbulence-related correction coefficients to simulate the combustion phasing using hydrogen-enriched ammonia laminar flame speed values. The results show that hydrogen enrichment accelerates both the early flame development and flame propagation phases due to enhanced chemical reactivity, leading to improved indicated mean effective pressure compared to neat ammonia. For a given excess air ratio, peak IMEP is achieved at 10% hydrogen addition by volume. The developed two-zone combustion model also captured the effects of exhaust gas recirculation through reduced flame speed and changes in thermodynamic properties. At 20% exhaust gas recirculation, nitric oxide emissions decreased by 48%, while the indicated specific fuel consumption increased by 10%.

1. Introduction

The utilization of ammonia is currently being investigated as a means of hydrogen storage. The main advantage of using ammonia is due to carbon-free combustion, a potential pathway for de-fossilization of the energy sector [1,2]. However, the usage of ammonia in combustion systems are challenging because of its narrow flammability limit and lower laminar flame speed (LFS) compared to gasoline. Additional challenges are due to its thermo-physical properties and poor oxidation characteristics of ammonia molecules that imposes resistance to hydrogen abstraction [3]. Ammonia powered SI engines also suffer from lower in-cylinder pressure compared to gasoline-fuelled SI engines, due to ammonia's lower energy content and slower flame speed [4]. The combustion characteristics of low-reactivity fuels like ammonia can be enhanced by adding a faster reactive fuel such as hydrogen or natural gas [5]. Hydrogen is carbon-free and it possesses advantageous combustion properties, including higher LFS, higher energy content, and a wide flammability range which could promote the ammonia flame stability [6,7]. Neat ammonia-fuelled SI engines require a significant reduction in induction lag to achieve complete and stable combustion [8], adding as little as 5% hydrogen by volume has been shown to reduce the SI engine induction lag by 5 ^{o}CA [9]. Hydrogen addition to ammonia SI engine improves not only the performance but also the combustion stability with minimal engine design changes [10]. Hydrogen addition has been demonstrated experimentally to improve ammonia premixed SI engine performance, but this benefit is limited by the reduction in volumetric efficiency; for a volumetric additions of 33% hydrogen the brake thermal efficiency improved by 17%, but suffered a 14% reduction in volumetric efficiency [11]. The performance of hydrogen enriched ammonia SI engine is comparable to that of methane by increasing the intake temperature and the in-cylinder turbulence intensity [12]. However, while hydrogen enrichment enhances ammonia combustion, it does not mitigate emissions concerns. Although ammonia combustion does not produce carbon dioxide, it generates significant nitrogen based emissions such as; nitrous oxide, nitrogen oxides, and unburned ammonia [13]. This is because of the presence of the nitrogen in the molecular structure of ammonia. When hydrogen is added to an ammonia SI engine, the higher flame speed and increased in-cylinder temperatures increases the nitrogen oxides emissions through both thermal NO and fuel NO mechanisms [14]. Therefore, controlling combustion temperatures is essential in hydrogen enriched ammonia SI engine to mitigate nitrogen oxide emissions [15]. An effective approach is to recirculate the exhaust gas EGR to reduce the nitrogen-based engine out emissions [16]. The EGR addition could be achieved by recycling a part of the exhaust gas into the intake flow, mixing it with the air intake

* Corresponding author.
E-mail addresses: Dardan.Rrustemi@brunel.ac.uk (D.N. Rrustemi), Thanos.Megaritis@brunel.ac.uk (T. Megaritis), Lionel.Ganippa@brunel.ac.uk (L.C. Ganippa).

https://doi.org/10.1016/j.fuel.2026.139124
Received 31 October 2025; Received in revised form 8 February 2026; Accepted 10 March 2026
Available online 18 March 2026

Nomenclature

Symbols

A	area (m^2)
C	constant
L	distance (m)
m	mass (kg)
N	engine speed (rpm)
P	in-cylinder pressure (MPa)
Q	heat transfer (J/degree)
T	in-cylinder temperature (K)
t	time (s)
U	internal energy (J)
u'	turbulence intensity (m/s)
S	speed (m/s)
V	volume (m^3)
θ	crank angle (degree)
ρ	density (kg/m^3)
λ	excess air ratio
τ	characteristic time (s)

Acronyms

AFR	air/fuel ratio
AHRR	apparent heat release rate (J/degree)
aTDC	after top dead centre
bTDC	before top dead centre
CA	crank angle
CA10	location of 10% mass fraction burned
CA50	location of 50% mass fraction burned
CA90	location of 90% mass fraction burned
EGR	exhaust gas recirculation
H_2	hydrogen
H_2O	water
ISFC	indicated specific fuel consumption (kg/kWh)
LFS	laminar flame speed (m/s)
MAP	manifold air pressure (kPa)
MFB	mass fraction burned
N_2	nitrogen
NH3	ammonia
NO	nitric oxide
O2	oxygen
SI	spark ignition
SL	flame speed
ST	spark timing
TDC	top dead centre

Subscripts

0	initial condition
b	burnt
d	displaced volume
e	entrained
f	flame
iv	intake valve lift
loss	heat losses
p	piston
soc	start of combustion
u	unburned
stoich	stoichiometric
T	Taylor microscale
τ	characteristic burning time (s)

[17]. The EGR composition of lean burn ammonia with hydrogen mixture consists of N_2, H_2O and O_2. The isolated addition of these species in the intake would have three prominent effects (i) thermal effect due to the increased heat capacity of the charge which would eventually decrease the in-cylinder temperature, (ii) dilution effect due to depletion of oxygen in the air intake, which decreases the in-cylinder mixture reactivity, and (iii) chemical effect accounting for third-body and radical-interaction effect due to H_2O addition [18]. Complementary to EGR addition, the hydrogen enriched ammonia SI engine could operate at lean burn conditions to further reduce nitric oxide emissions and to improve thermal efficiency [10]. However, the ammonia combustion under lean burn condition is particularly sensitive to turbulence-chemistry interactions, as the ammonia flames are typically characterized by wrinkled and corrugated flame structure that occurs at the boundary between a thin reaction zones, where the flame stretch and local quenching can destabilise the combustion [19]. To capture the turbulence-chemistry interactions effect in flame propagation, detailed reaction rate mechanism of ammonia with hydrogen combustion and flame speed are essential for modelling. Recently a dedicated kinetic mechanism of ammonia with hydrogen was developed through evaluation of reaction pathways and species thermochemistry, which was validated against experimental ignition delay, laminar flame speeds, and speciation data across a wide range of operating conditions [20]. This kinetic mechanism identified the dominant reaction pathways at temperatures greater than 1500 K and at intermediate temperature between 1000 to 1500 K, as well as nitrogen oxides formation. The accuracy of 16 reaction mechanisms for ammonia/hydrogen combustion has been quantitatively assessed by comparing experimental data with reaction mechanism predictions for species concentrations, ignition delays, and laminar burning velocities [21]. Since the fundamental kinetics of ammonia with hydrogen combustion is developed in [20], the LFS under various engine-relevant conditions can be calculated from these detailed chemical kinetic simulations. These LFS values can then be used as inputs to simplified thermodynamic combustion modelling approaches. The need for a detailed and complex turbulence sub-models in SI engines can be circumvented by applying turbulence scaling to the flame area, to simulate mass fraction burn (MFB) [22]. Once the simulated MFB values are optimised to match the thermodynamic practical engine experimental data at 10%, 50%, and 90% burned mass fraction, the model may be capable of predicting key engine parameters such as in-cylinder pressure and temperature with high degree of accuracy [23]. The complex multi-dimensional models with high spatial accuracy are widely used in industry but they are time consuming and not as cost effective as global zero-dimensional combustion models [24]. The two-zone combustion model allows the separation of burned and unburned gas regions, allowing the incorporation of fuel-specific effects like LFS, and thermophysical properties which are important for modelling dual-fuel combustion [25]. The two-zone combustion model could accurately capture the hydrogen addition influence on the flame speed, combustion phasing, and efficiency across various engine operating conditions by using the LFS, and turbulence effects [26]. Hydrogen addition effect could also be captured by incorporating a fractal dimension that adjusts turbulent flame surface growth based on hydrogen concentration, allowing to predict the combustion behaviour across different operating and blending conditions [27]. The two-zone combustion model could be an effective tool to predict the performance of turbulent premixed combustible mixtures through the effective incorporation of LFS, mixture thermodynamic state properties and turbulence intensity. The contribution of this work is the implementation of correction constants to entrainment-based mass fraction burn model to accurately predict combustion phasing in hydrogen-enriched ammonia SI engine. This methodology effectively eliminates the limitations of zero-dimensional formulations that require combustion phasing, which is influenced by spatial in cylinder turbulence. Then this entrainment-based mass

fraction burn model was then integrated into a two-zone combustion model to predict the performance of hydrogen enriched ammonia SI engine for various operating conditions under exhaust gas recirculation environment.

2. Methodology

An entrained based two-zone combustion model was used to predict the performance of an ammonia fuelled SI engine under various percentages of hydrogen addition, excess air ratios, spark timings, manifold air pressures, and exhaust gas recirculation rates. The main assumption of the combustion model is the division of the combustion chamber into two zones: the unburned zone and the burned zone. The unburned zone consists of the reactants, such as ammonia and air, with varying concentrations of hydrogen and exhaust gas compositions, whereas the burned zone consists of the products resulting from the combustion of these reactants. Both the unburned and burned zones are treated as ideal gases, and it is assumed that there is no heat transfer between the two zones. This simplification may lead to a slight overprediction of unburned-zone temperatures and an underestimation of interfacial heat losses. The pressure is assumed to be uniform throughout the chamber, while the temperature differs between the unburned and burned zones. In addition, the model does not resolve spatial inhomogeneities of the change in the cylinder, which may lead to a slight underprediction of the overall indicated efficiency. The governing equations of the combustion model are shown in Appendix A3.

2.1. Simulation conditions

The excess air ratio for ammonia with hydrogen combustion is defined as:

$$\lambda = \frac{\left(\frac{x_{NH_3}+x_{H_2}}{x_{air}}\right)_{stoich}}{\left(\frac{x_{H_2}+x_{NH_3}}{x_{air}}\right)_{act}} \tag{1}$$

where the x_{H_2}, x_{NH_3} and x_{air} are the mass of hydrogen, ammonia, and air, respectively. The subscripts *stoich* and *act* denote the stoichiometric and actual mixtures of air and fuel. The stoichiometric air-to-fuel ratios of ammonia and hydrogen are 6.05 and 34, respectively. The operating conditions chosen for this study are presented in Table 1. For a given intake pressure, the intake air mass was fixed, and the ammonia mass was adjusted according to the hydrogen addition percentage to maintain a constant excess air ratio. The EGR composition consists of the combustion products such as H_2O and N_2 under stoichiometric conditions. For lean-burn mixtures ($\lambda > 1$), unreacted O_2 was also included in the EGR composition, as shown in Appendix A1.

2.2. Laminar flame speed and mass fraction burned model

The laminar flame speed (LFS) data is essential to characterize the hydrogen enrichment effect on ammonia combustion in SI engines. The experimental data for ammonia with hydrogen combustion under high pressures engine-relevant conditions are scarce due to flame instabilities [28]. The Converge software was used to determine the LFS based on the chemical kinetic mechanism proposed in [20]. The LFS of hydrogen-enriched ammonia mixtures is incorporated into the two-zone combustion model, which was formulated by introducing an entrained zone that interfaces with the unburned and burned zones [29], as shown in Fig. 1. The flame kernel that evolves from the spark develops and interacts with in-cylinder turbulence, undergoing intensive stretching and wrinkling due to turbulence. After a transition period, the propagating flame becomes fully turbulent. As the flame expands, the entrainment of the unburned zone increases, causing the flame to advance faster than the rate at which combustion actually takes place [30]. The difference between the entrainment rate and the burning rate is characterized by a characteristic eddy burn time, τ_C. The entrained mass fraction of the unburned zone and the actual mass fraction burned were calculated based on Equations (2) and (3), respectively.

$$\frac{dm_e}{dt} = \rho_u A_f (S_l + u') \tag{2}$$

$$\frac{dm_b}{dt} = \frac{m_e - m_b}{\tau_C} \tag{3}$$

where m_e is the entrained mass, m_b is the burned mass, ρ_u is the unburned mixture density,A_f is the mean flame front area, S_L is the hydrogen enriched ammonia laminar flame speed, and u' is the in-cylinder turbulence intensity. The mean flame front area A_f was calculated based on a predictive approach proposed in [31]. The characteristic burning time, τ_C, was determined as the ratio of the Taylor micro-scale length L_T to the laminar flame speed S_L corrected by a factor, C_τ, which is given as:

$$\tau_C = \frac{L_T}{S_L} \tag{4}$$

The Taylor micro-scale length,

$$L_T = 0.8 L_{iv} \left(\frac{\rho_0}{\rho_{st}}\right)^{\frac{1}{3}} \tag{5}$$

was calculated as discussed in [26], where L_{iv} is the intake valve lift, and, ρ_0 and ρ_{st} are the in-cylinder mixture density at the intake and spark timing, respectively. The turbulence intensity u' was calculated as discussed in [29],

Table 1
Operating conditions used in the numerical model.

Parameters	Values
Spark Timing (°CA bTDC)	50 to 0
Excess air ratio (−)	1 to 1.5
MAP (kPa)	90 to 130
Hydrogen addition (% by volume)	0 to 60
Exhaust gas recirculation (% by volume)	0 to 20

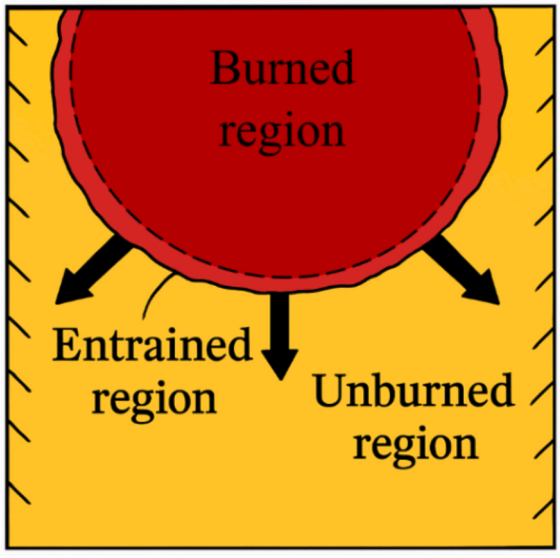

Fig. 1. Schematic of the combustion model illustrating the entrained, burned and unburned zones.

$$u' = C_{u'} S_p \left(\frac{\rho_{st}}{\rho_0}\right)^{\frac{1}{3}} \quad (6)$$

where $C_{u'}$ is the experimental validation constant to correct u', S_p is the mean velocity of the piston. The Nelder–Mead simplex algorithm was used to find the correction constants that shift the simulated MFB closer to the experimental combustion phasing. The optimization through minimisation of an objective function was defined as the total squared error between the simulated and experimental combustion phasing, as described below:

$$\in (c) = \sum_{i=3}^{3} \left(CA_{sim,i}(c) - CA_{exp,i}(c)\right)^2 \quad (7)$$

where c indicates the correction constants, and i indicates the CA10, CA50 and CA90 locations for the respective engine operating conditions.

3. Results and discussion

3.1. Ammonia with hydrogen enrichment laminar flame speed

Laminar flame speed significantly influences combustion stability and flame propagation in ammonia-based fuel blends [32]. To obtain a fundamental understanding of the effect of hydrogen addition on the LFS of ammonia combustion, the LFS under engine relevant conditions were calculated for ammonia with hydrogen using the chemical kinetic mechanism [20]. Fig. 2 compares the simulated and experimental LFS values of ammonia with various hydrogen addition percentages at elevated temperatures at a pressure of 1 atm. Under all presented conditions, the LFS increases monotonically with increasing temperature, which is consistent with the Arrhenius-type dependence of reaction rates [28]. It can be seen that hydrogen addition enhances the reactivity of the ammonia mixture, particularly at higher temperatures. This trend is well captured by the ammonia with hydrogen reaction kinetic mechanism proposed in [20], which shows good qualitative agreement with the experimental LFS data reported in [32]. At an excess air ratio of 1, the ammonia LFS increased by nearly fivefold as the temperature increased from 500 to 800 K (Fig. 2a). At 700 K, for an excess air ratio of 1, the LFS of ammonia increased by 61%, 212%, and 469% with hydrogen additions of 20%, 40%, and 60% by volume, respectively. This enhancement is attributed to hydrogen's high diffusivity, wide flammability limits, and strong radical-generating capability [33]. Overall, the simulated LFS values show good agreement with the experimental data, with slight deviations observed for ammonia containing 20% and 40% hydrogen. Where, the chemical reaction kinetic mechanism tends to slightly underpredict the LFS at higher temperatures; however, the deviation remains within the reported experimental uncertainty [32]. Furthermore, as the excess air ratio increases, the LFS decreases due to the reduced energy input. At a temperature of 800 K, the LFS of ammonia with 60% hydrogen addition decreased by 21% as the excess air ratio increased from 1.0 to 1.25, consistent with the experimental findings of [32]. Fig. 3 shows the variation of ammonia LFS at various temperatures for different excess air ratios and for different hydrogen volumetric fractions of 0% (Fig. 3a), 20% (Fig. 3b), 40% (Fig. 3c), and 60% (Fig. 3d) at a pressure of 1 MPa, which was chosen based on the in-cylinder pressure closer to spark timing. It could be observed that for all hydrogen additions, the LFS increases monotonically with increasing unburned mixture temperature, consistent with the Arrhenius-type temperature dependence of reaction rates [28]. Under the stoichiometric condition (excess air ratio of 1) for a hydrogen addition of 60%, the LFS increases by more than five times when the temperature increased from 450 K to 800 K as shown in Fig. 3d. This shows a significant enhancement in chemical reactivity because of combined effect of temperature and hydrogen enrichment of ammonia mixture. Hydrogen addition significantly increased the LFS of ammonia-air mixtures, especially at higher temperatures. At a temperature of 700 K and for an excess air ratio of 1.2, increasing the hydrogen addition from 0% to 60% increases the LFS from 0.19 m/s to 1.1 m/s, marking an increase of 479%. This effect was because of the higher reactivity, diffusivity, wider range of flammability, higher flame speed, and radical-generating capacity of hydrogen, which accelerates the overall combustion kinetics of the hydrogen and ammonia blends [33]. Fig. 4 shows the LFS of ammonia with various percentages of hydrogen addition at different exhaust gas recirculation (EGR) rates. The reactive mixture was maintained at an excess air ratio of 1.2 and at a pressure of 1 MPa. The mixture composition of EGR varied at different excess air ratios and hydrogen addition percentages, as shown in Appendix A1. It can be seen that in this work the addition of EGR composed of H_2O and N_2 under stoichiometric conditions and for lean burn mixtures ($\lambda > 1$), unreacted O_2 was also included in the EGR composition, to the

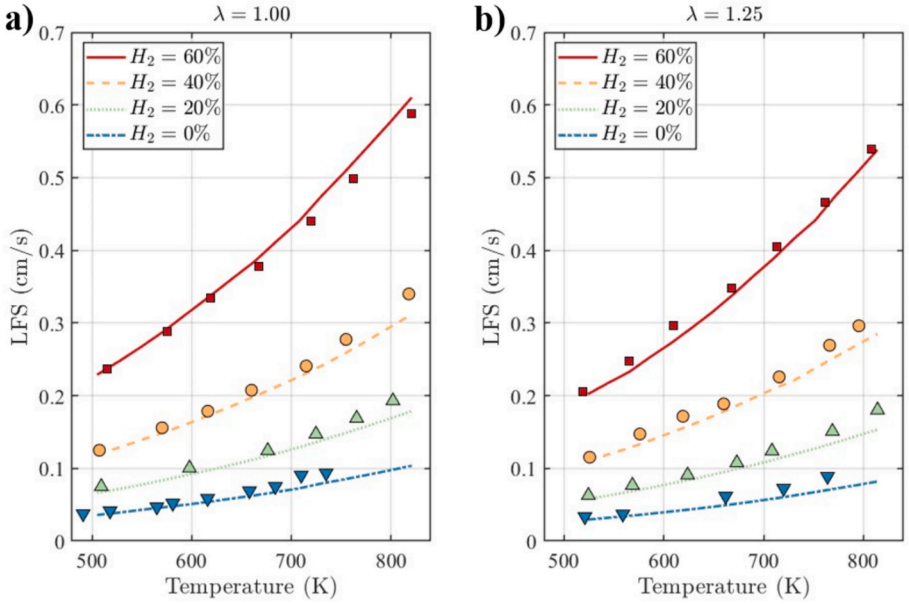

Fig. 2. Simulated laminar flame speed values using the reaction kinetic mechanism of [20] compared with the experimental data of [32] for a) an excess air ratio of 1 and b) an excess air ratio of 1.25, at various hydrogen additions and temperatures at a pressure of 1 atm.

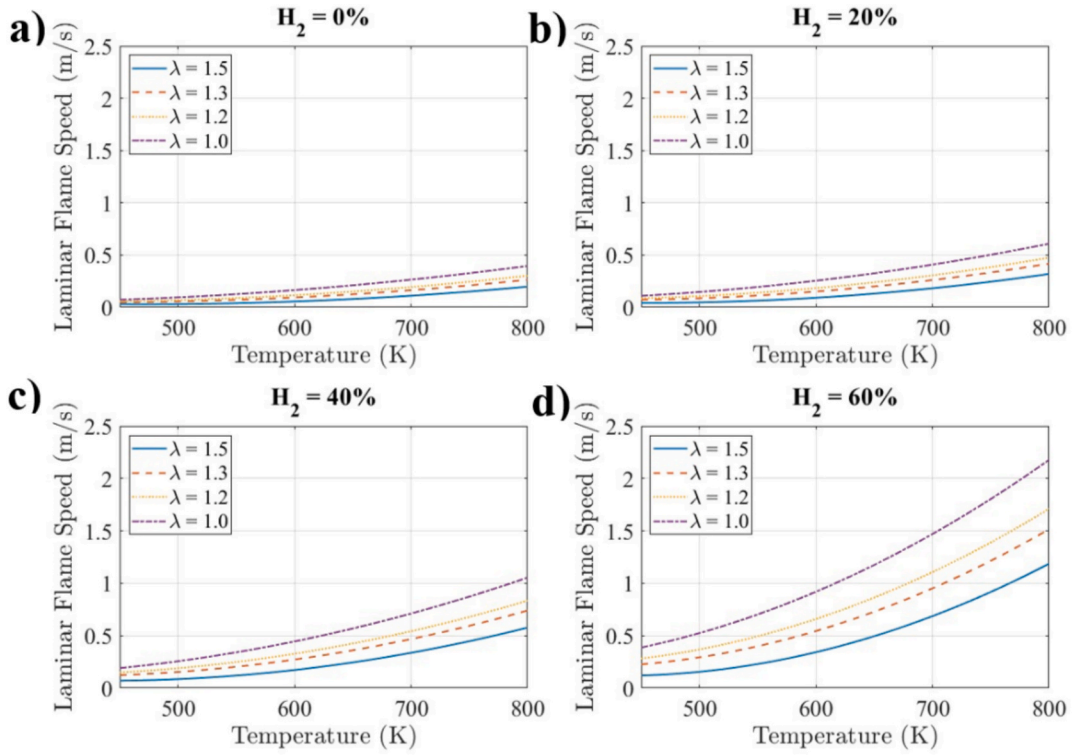

Fig. 3. The LFS for mixtures of ammonia with different percentages of hydrogen maintained at different excess air ratios at a pressure of 1 MPa at different temperatures. Calculated using chemical kinetics with the mechanism of [20].

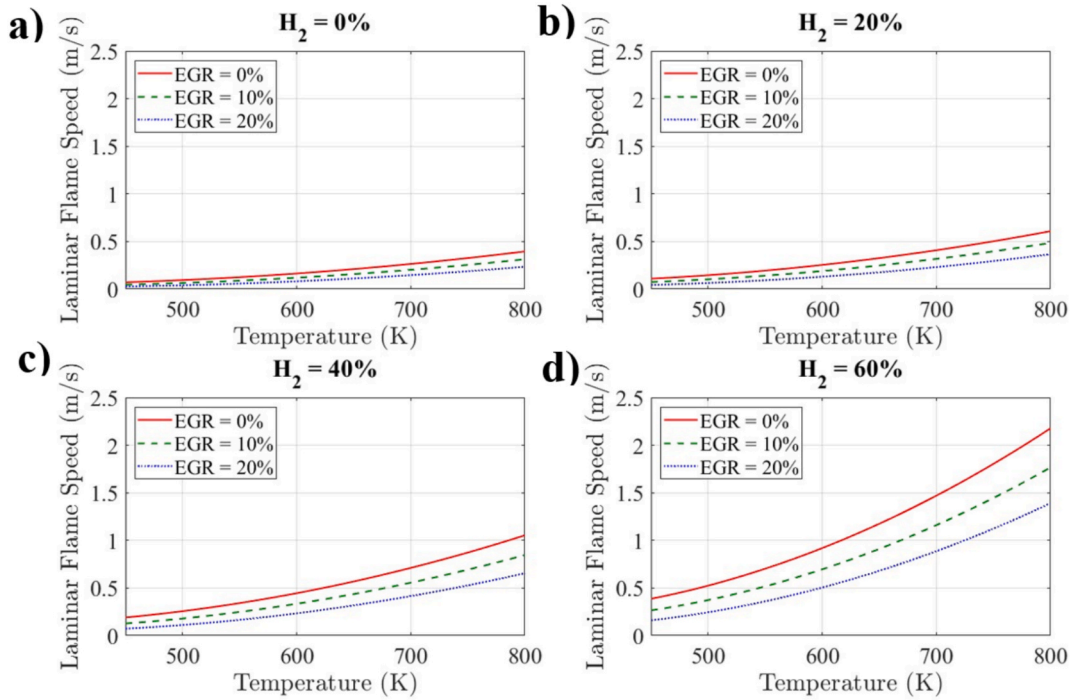

Fig. 4. The LFS of ammonia at different percentages of hydrogen at different temperatures and EGR rates maintained at an excess air ratio of 1.2 and at a pressure of 1 MPa. Calculated using chemical kinetics with the mechanism of [20].

ammonia-air mixture with various percentages of hydrogen addition led to a notable reduction in the LFS. For neat ammonia at an excess air ratio of 1.2 at a pressure and temperature of 1 MPa and 700 K, the LFS decreased by 23%, and 44% as the EGR rate increased from 0% to 10%, and 20%, respectively. This decrease of the flame speed was mainly because of the thermal effect of EGR that reduces the adiabatic flame temperature due to its high specific heat capacity of the mixture, and the dilution of the charge reduces the concentration of reactive radicals that are essential for chain-branching reactions. The addition of EGR decreased the burning velocity by attenuating the concentration of OH

radicals. The LFS results highlight the importance of hydrogen enrichment in enhancing the flame propagation in ammonia fuelled engines. Furthermore, it could be seen that the LFS is sensitive to variations in temperature, excess air ratio, and addition of EGR. All of these variations have been accurately accounted in the two-zone modelling of ammonia-air mixtures with hydrogen enrichment combustion under high pressure engine environment. Fig. 5a shows the LFS sensitivity analysis for a stoichiometric ammonia mixture with different hydrogen addition percentages, maintained at an unburned temperature of 700 K and a pressure of 1 MPa. The positive LFS sensitivity coefficients of various reactions of species indicate that those reactions increase the mixture reactivity. For neat ammonia and for low hydrogen addition percentage, the H atoms are mainly produced by NNH decomposition reactions such as: NNH=H + N_2 and NH + NH_2=H + N_2H_2, and by the NNH formed from NH_2 + NO=NNH + OH. Whereas for ammonia-air mixtures with higher hydrogen addition percentages of 40% and 60%, the main production of H atoms was through hydrogen abstraction by O and OH through the reactions H_2 + O=H + OH and H_2 + OH=H + H_2O, respectively, which increases the reactivity via H + O_2=O + OH. In contrast, the negative LFS sensitivity coefficients of various species reactions indicate that the reactions decrease the mixture reactivity. The reaction H + N_2H_2=H_2 + NNH reduces reactivity across all hydrogen addition levels by consuming H radicals, thereby limiting their availability for key chain-branching reactions such as H + O_2=O + OH. However, for ammonia with hydrogen addition, the sensitivity of this reaction the flame speed increases, as the quantity of H radicals increased with hydrogen enrichment in the ammonia mixtures. Both NH_2 + NO=H_2O + N_2 and NH_2 + O=H + HNO decreased reactivity by producing stable NO or HNO (a NO precursor), which do not contribute to radical propagation. Moreover, it can also be seen from Fig. 5a that the decomposition reaction; NH_3 + M=NH_2 + H + M decreased reactivity mainly due to being endothermic and slow. The reaction H + O_2(+M)=HO_2(+M) shows the greatest sensitivity magnitude in decreasing the reactivity for ammonia with greater than 20% hydrogen addition percentages. This was because that the formation of intermediates such as HO_2 acts as a radical sink. As the hydrogen addition percentage increased, the sensitivity of H + O_2(+M)=HO_2(+M) reaction also increased, as it diverted H radicals away from the reaction H + O_2=O + OH. It can also be seen from Fig. 5b and c that when EGR was added to ammonia with or without hydrogen addition, the sensitivity of LFS due to reaction H + O_2(+M)=HO_2(+M) decreased with EGR due to more third bodies absorbing energy at higher H_2O formation. The increase of the third-body collisions reduced the temperature, and thereby decreasing flame speed. With EGR addition, the presence of H_2O may also promote HO_2 formation, creating a low-reactivity radical pool. It can be observed that the reaction NH_2 + NO=H_2O + N_2 has negative sensitivity on LFS for neat ammonia, and this effect increased with EGR addition due to participation of NH_2 and NO as active species in ammonia oxidation and their conversion into stable H_2O and inert N_2. However, this effect was not significant in Fig. 5 for ammonia with 60%

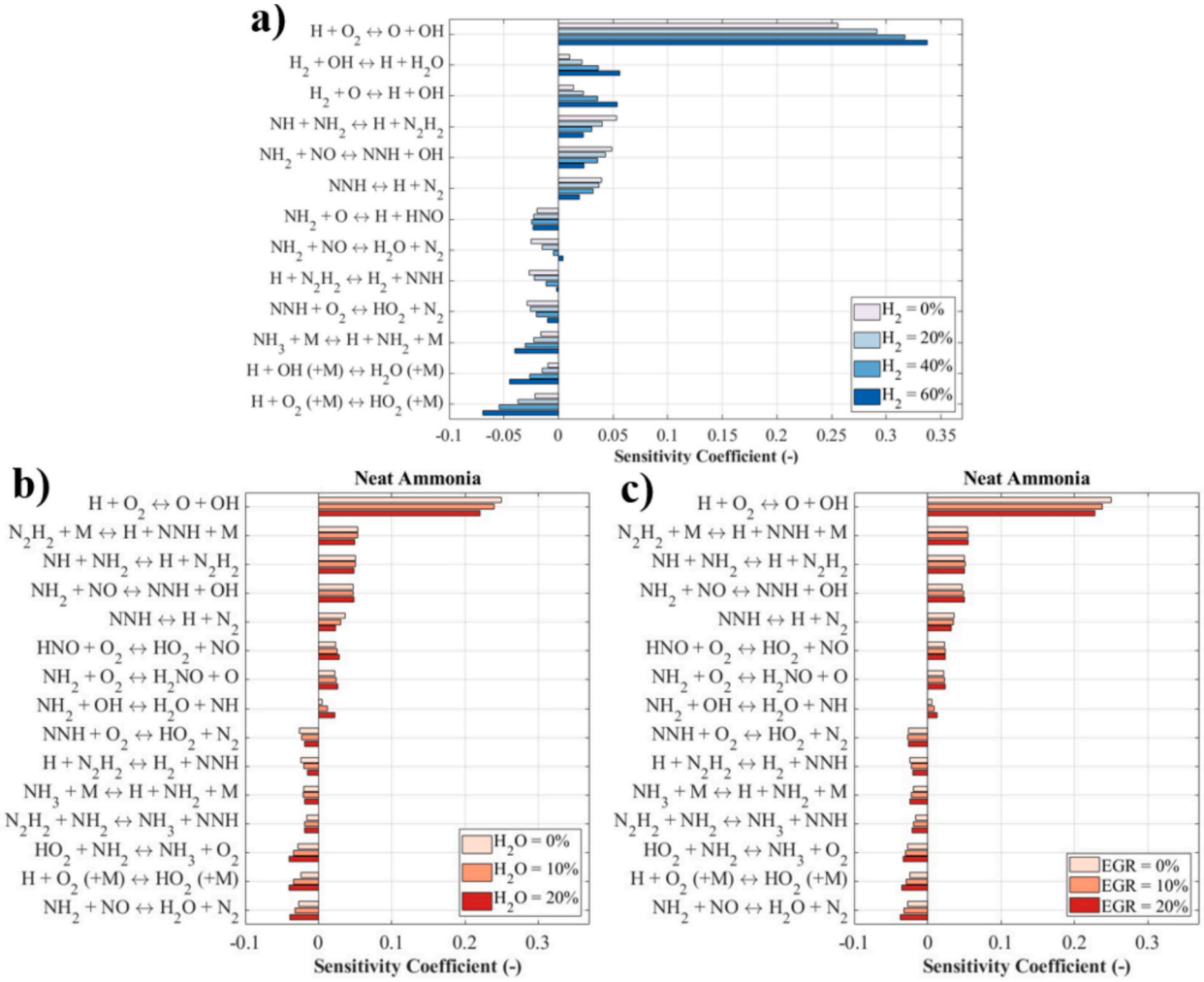

Fig. 5. Flame speed sensitivity analyses for a) ammonia with different hydrogen addition percentages, b) neat ammonia with different EGR addition percentages, and c) ammonia with 60% hydrogen addition with different EGR addition percentages (Tu = 700 K, P = 1 MPa, λ = 1).

hydrogen addition, with or without EGR, due to the high temperature and H radical rich environment caused by hydrogen addition, under which the reactions tend to become exothermic.

3.2. Validation of mass fraction burned and two-zone combustion model

The proportion of the fuel burnt in the combustor was calculated based on the entrained mass fraction burn model presented in Eq. (3), which is strongly influenced by the eddy characteristic burning time, τ_C, and the turbulence intensity, u'. Since the combustion of ammonia with hydrogen addition is affected by in-cylinder flame-induced turbulence, the modelling of turbulence effect on flame is important. In this study, the zero-dimensional models were incorporated with correction factors C_τ and $C_{u'}$ to account for the turbulence effect, and they were fitted to match the experimental data. The eddy characteristic burning time, τ_C, was calculated as the ratio of the Taylor microscale to the LFS, corrected by a factor C_τ. The correction constant C_τ was fitted using linear regression between the Taylor microscale and the LFS, calculated from Eq. (4). Meanwhile, the turbulence intensity was modelled based on mean piston speed and variations in in-cylinder density ratio, corrected by a factor $C_{u'}$. The correction constant $C_{u'}$ was fitted through linear regression between the turbulence intensity, calculated from Eq. (5), and the LFS at various hydrogen additions, equivalence ratios, and spark timings. In Fig. 6, the corrected and uncorrected stoichiometric ammonia mass fraction burned are shown in comparison with experimental data at various percentages of hydrogen addition and spark timings. The uncorrected mass fraction burned deviates significantly from the CA10, CA50, and CA90 experimental data. This signifies the importance of incorporating the correction factor C_τ and $C_{u'}$ to correct the characteristic burn time and turbulence intensity with experimental data by accounting for the coupling between the in-cylinder flow and combustion chemistry in two-zone combustion model. For uncorrected ammonia with 0% and 20% hydrogen addition, the model overpredicts CA10, CA50, and CA90 due to its inability to capture the spatial inhomogeneities of low reactivity of ammonia. For ammonia with 60% hydrogen addition, the uncorrected model underpredicts CA10, CA50, and CA90 because it cannot capture the significantly increased mixture reactivity with hydrogen addition. However, it could be seen that the corrected mass fraction burned was able to capture the effect of hydrogen addition at CA50 and CA90 because the correction factors for C_τ and $C_{u'}$ accounted for the turbulence–flame interaction and changes in ammonia mixture reactivity with hydrogen addition. However, it can be seen from Fig. 6 that, even with the correction constants, there is still a deviation in the prediction of the CA0–10 phase. The limited accuracy of the model in the CA0–10 phase is mainly due to the lack of a flame kernel growth sub-model, as the early flame development phase is governed by spatio-temporal variations of the charge in the near vicinity of spark plug, which could not be captured by the proposed entrained based mass fraction burn model. The resulting mass fraction burn data is used as input to the two-zone combustion model to predict the performance of the hydrogen-enriched ammonia SI engine under various operating conditions. The simulated values of the in-cylinder pressure of ammonia at different hydrogen additions, excess air ratios and spark timings from the proposed two-zone combustion model were validated

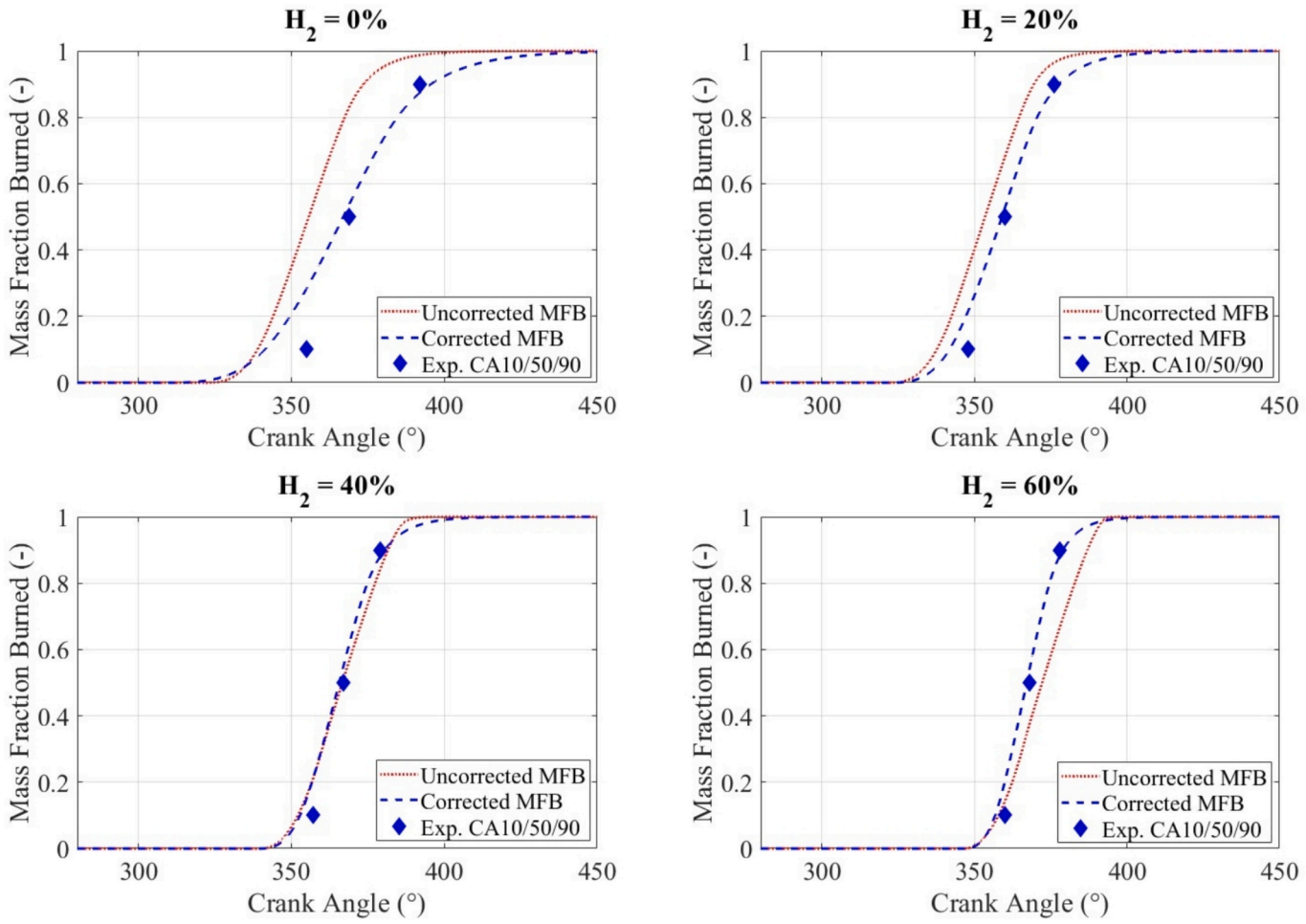

Fig. 6. Stoichiometric ammonia uncorrected and corrected mass fraction burned compared to experimental data at various hydrogen additions, and spark timings. Experimental data [10].

using published experimental data [10]. In Fig. 7, the red line and red markers represent the simulated and experimental in-cylinder pressure values for the neat ammonia SI engine operation at stoichiometry, while the blue line and blue markers represent the simulated and experimental in-cylinder pressure values for ammonia with 40% hydrogen addition. The presented in-cylinder pressure data shows that the developed two-zone combustion model based on LFS and MFB based on C_τ and $C_{u'}$ is able to capture the effect of hydrogen addition on ammonia combustion in an SI engine at various operating conditions. The results show a slight overprediction during the early stages of combustion in all presented cases. The variations between the experimental in-cylinder pressure data and the two-zone combustion model results were quantified, and the standard error was found to be within 4% for both 0% and 40% hydrogen addition conditions, with a maximum deviation of 0.11 MPa and 0.15 MPa for 0% and 40% hydrogen addition, respectively. The differences between the experimental and simulated in-cylinder pressure were caused by the slight overprediction of corrected MFB of CA10 for ammonia with hydrogen combustible mixtures, as discussed in Fig. 6. This was because of the prolonged induction lag of neat ammonia and hydrogen-enriched ammonia mixture due to lower LFS values. Also, the experimental uncertainties due to cycle-to-cycle fluctuations under hydrogen enrichment and the associated stability of ammonia flames cannot be ignored for the early flame kernel development phase [10]. Based on the in-cylinder pressure results shown in Fig. 7 it can be seen that the developed two-zone combustion model with the incorporated LFS and MFB predicts the combustion characteristics of hydrogen-enriched ammonia SI engine with a standard error of less than 4%.

3.3. Combustion characteristics

3.3.1. Indicated mean effective pressure

The developed two-zone model incorporated with LFS and modified MFB was used to simulate the ammonia SI engine combustion performance at a spark timing that corresponds to the minimum spark advance for best torque (MBT) to ensure the highest thermal efficiency. The MBT timing was determined by varying the spark timing and identifying the condition that produced the highest indicated mean effective pressure (IMEP) at a particular excess air ratio, manifold air pressure and hydrogen addition. It can be seen from Fig. 8a that the MBT timing shifts closer to top dead centre (TDC) when hydrogen was added to ammonia combustion. For an excess air ratio of 1.2 the MBT shifted from 34 °CA bTDC to 28 °CA bTDC, 26 °CA bTDC and 19 °CA bTDC for 10%, 20%, and 40% hydrogen additions. This was because the hydrogen enrichment accelerates combustion, therefore a shorter combustion duration due to higher diffusivity of hydrogen and its higher LFS [33]. The enrichment of hydrogen to ammonia-air mixtures causes the spark timing to be retarded for higher IMEP. It could also be seen from Fig. 8b, that for neat ammonia operation at a fixed MAP, the IMEP decreases when the mixture becomes leaner. For a fixed spark timing at 30 °CA bTDC the IMEP decreased by 11%, 18%, and 32% when the excess air ratio was changed from 1 to 1.2, 1.3 and 1.5, respectively. This decrease in IMEP with increased air dilution was due to the reduction of LFS for leaner mixtures. The excess air in the combustible mixture also lowers the flame temperature and the OH radical concentration, thereby reducing the reaction rate of $H + O_2 = O + OH$ [34]. This effect has been effectively captured by the two-zone combustion model through the incorporation of LFS, which was calculated for the hydrogen-enriched ammonia mixtures through chemical kinetic detailed reaction mechanism [20]. This reduction in the flame speed for higher air diluted ammonia mixtures causes the MBT timing to be shifted further away from TDC, as more time is required for these ammonia mixtures to complete combustion. For the neat ammonia combustion under a MAP of 110 kPa, the MBT shifted from 31 °CA bTDC to 34 °CA bTDC, 43 °CA bTDC, and 48 °CA bTDC when the excess air ratio was changed from 1 to 1.2, 1.3 and 1.5, respectively. Fig. 8c shows the variation of the neat ammonia IMEP at various spark timings for a fixed excess air ratio of 1.2 at various manifold air pressures. As the manifold air pressure increased, the MBT timing shifted slightly away from TDC due to the increased amount of charge to be burned, which increased the charge density inside the chamber. For a fixed spark timing of 30 °CA bTDC and at an excess air ratio of 1.2, the IMEP increased by 21% and 37% when MAP was increased from 90 kPa to 110 kPa and 130 kPa, respectively. Once the MBT was identified for each mixture condition of ammonia with hydrogen addition at various excess air ratios and manifold air pressures, the IMEP was simulated for the operating conditions presented in Table 1. It can be seen from Fig. 9a that the IMEP of ammonia powered SI engine initially increases with hydrogen addition up to 10% by volume, because of the higher flame speed of hydrogen and its lower

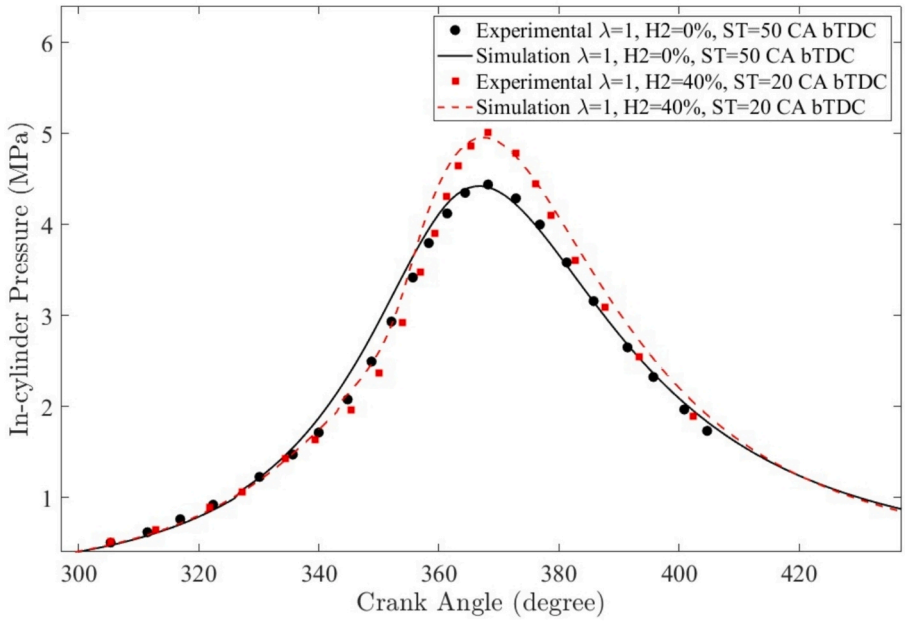

Fig. 7. The simulated in-cylinder pressure compared to experimental values of [10] (MAP = 120 kPa, CR = 10.5, N = 1500 rpm, $ST_{X_{H_2=0}}$=50 °CA bTDC, $ST_{X_{H_2=0.4}}$=20 °CA bTDC).

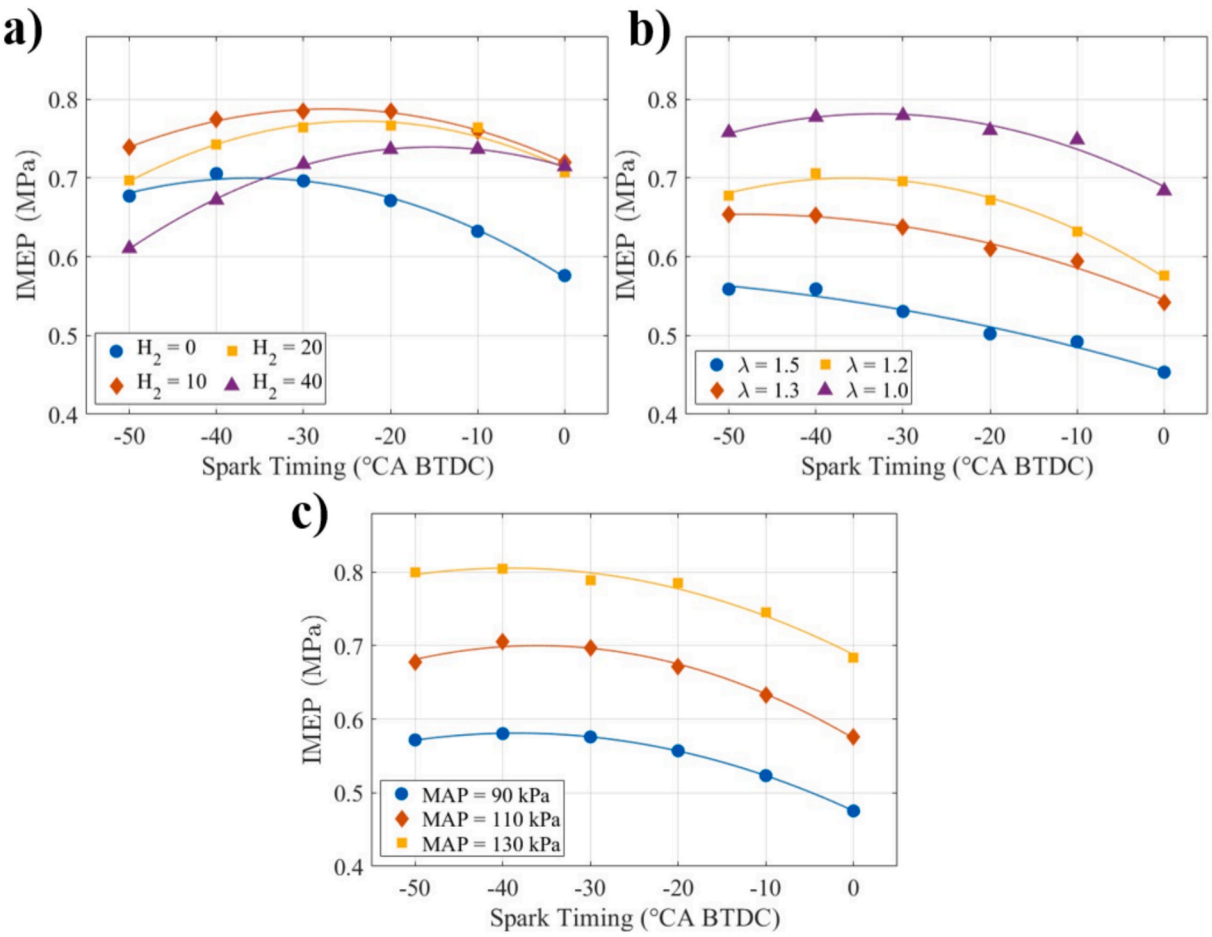

Fig. 8. a) Simulated IMEP at various spark timings and hydrogen addition (MAP = 110 kPa, λ=1.2), b) simulated IMEP at various spark timings and excess air ratios for neat ammonia (MAP = 110 kPa, x_{H_2}=0), and c) simulated IMEP at various spark timings and manifold air pressures (λ = 1.2, x_{H_2}=0).

heating value compared to neat ammonia, similar effect was observed in [9]. It could also be seen that for hydrogen additions beyond 10%, the IMEP decreased for ammonia SI engine. This phenomenon was consistently observed under all presented excess air ratios in Fig. 9a where the ammonia SI engine reached a peak at 10% addition of hydrogen. For the stoichiometric neat ammonia combustion, the load was 0.78 MPa, 0.86 MPa, 0.90 MPa, and 0.89 MPa, 0.88 MPa, 0.85 MPa, and 0.83 MPa for 0%, 5%, 10%, 15%, 20%, 40%, and 60% hydrogen additions respectively. The decrease in IMEP for hydrogen additions above 10% in the ammonia SI engine was due to the reduction in ammonia mass required to maintain a constant excess air ratio. Since hydrogen has a much higher stoichiometric air–fuel ratio than ammonia, its addition resulted in a very slight increase in the total fuel energy input from 236 J to 240 J for neat ammonia and ammonia with 60 hydrogen addition percentage, respectively. However, the increased hydrogen fraction raised the in-cylinder temperature due to the quicker combustion of hydrogen compared to ammonia, because of the increased chemical reactivity through the reaction $H + O_2 = O + OH$, with O and OH supplied by $H_2 + O = H + OH$ and $H_2 + OH = H + H_2O$. This led to a greater temperature difference between the in-cylinder charge and the chamber walls, which caused a reduction in IMEP. This observation lines with the experimental work on hydrogen-enriched ammonia SI engines [10,28]. It should also be noted that, even though the IMEP peaked at 10% hydrogen addition, the IMEP values for 20%, 40%, and 60% hydrogen additions decreased respectively, but still remained higher than that of the neat ammonia SI engine, showing the beneficial combustion enhancing properties of hydrogen addition to ammonia mixtures. Fig. 9a shows that IMEP decreases with increasing excess air ratio. For ammonia with 10% hydrogen addition, the IMEP dropped by 12%, 16%, and 26% as excess air ratio increased from 1 to 1.2, 1.3, and 1.5, respectively. This reduction is attributed to the lower fuel quantity in more air-diluted mixtures. In contrast, the application of EGR resulted in a reduction of IMEP across all presented operating conditions shown in Fig. 9b. For the neat ammonia SI engine, the IMEP decreased by 16% and 31% with 10% and 20% EGR addition by volume, respectively. This reduction in IMEP due to EGR was accurately captured by the developed two-zone combustion model through the LFS values calculated using the chemical kinetic mechanism under various operating conditions. The LFS decreases due to the dilution effect of EGR, which reduces oxygen availability and lowers the overall chemical reaction rates, thereby slowing down the combustion process. Finally, the flame speed reduction and variation of thermodynamic properties of the hydrogen enriched ammonia combustible mixture explains the observed decline in IMEP with increasing EGR rates. As it could be seen that the in-cylinder pressure in Fig. 10a for neat ammonia and Fig. 10b for ammonia with 60% hydrogen addition decreases with the composition of species that corresponds to 20% EGR. For the neat ammonia, the maximum in-cylinder pressure decreases from 3.9 MPa to 2.8 MPa, and for ammonia with 60% hydrogen addition it decreased from 5 MPa to 3.5 MPa for 20% EGR addition. To investigate the isolated effects of thermal, chemical, and dilution mechanisms associated with EGR addition on the combustion characteristics a decoupling approach was adopted within the two-zone combustion model, allowing each contribution to be evaluated independently under identical operating conditions. The thermal effect accounts for variations in the specific heat ratio, calculated using temperature-dependent thermodynamic properties derived

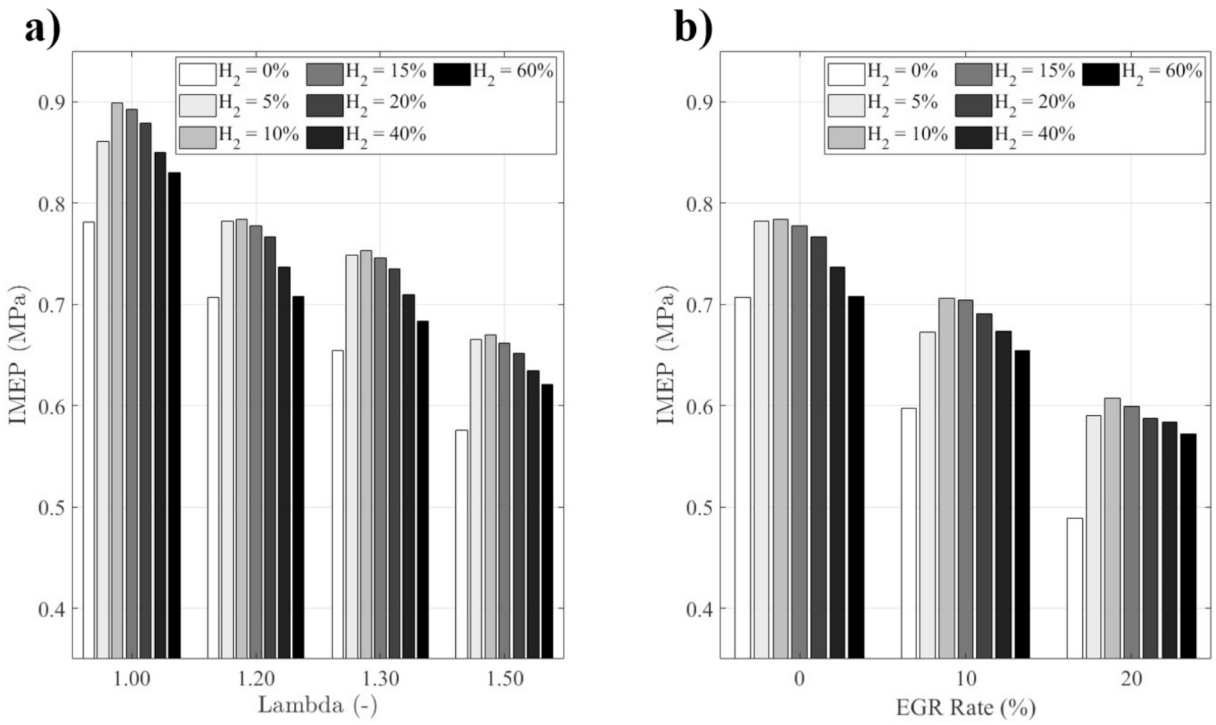

Fig. 9. a) Simulated IMEP at various hydrogen additions and excess air ratios (MAP = 110 kPa), and b) simulated IMEP at various hydrogen additions and EGR rates (λ = 1.2, MAP = 110 kPa).

from NASA polynomials, together with the reduction in LFS caused by the decrease in mixture temperature resulting from the addition of species such as water, nitrogen, and oxygen under lean-burn conditions. It should be noted that the reduction in LFS with EGR addition reflects the combined influence of thermal cooling and dilution of the reactive mixture, evaluated under a non-reactive dilution assumption without introducing additional chemical interactions. The resulting LFS was then incorporated into the two-zone combustion model. Whereas the chemical effect of EGR was evaluated by accounting only for chemistry-related influences such as third-body and radical interaction effects on the LFS, while excluding thermal effects. Finally, the dilution effect of EGR was quantified by considering the increased fraction of dilution in

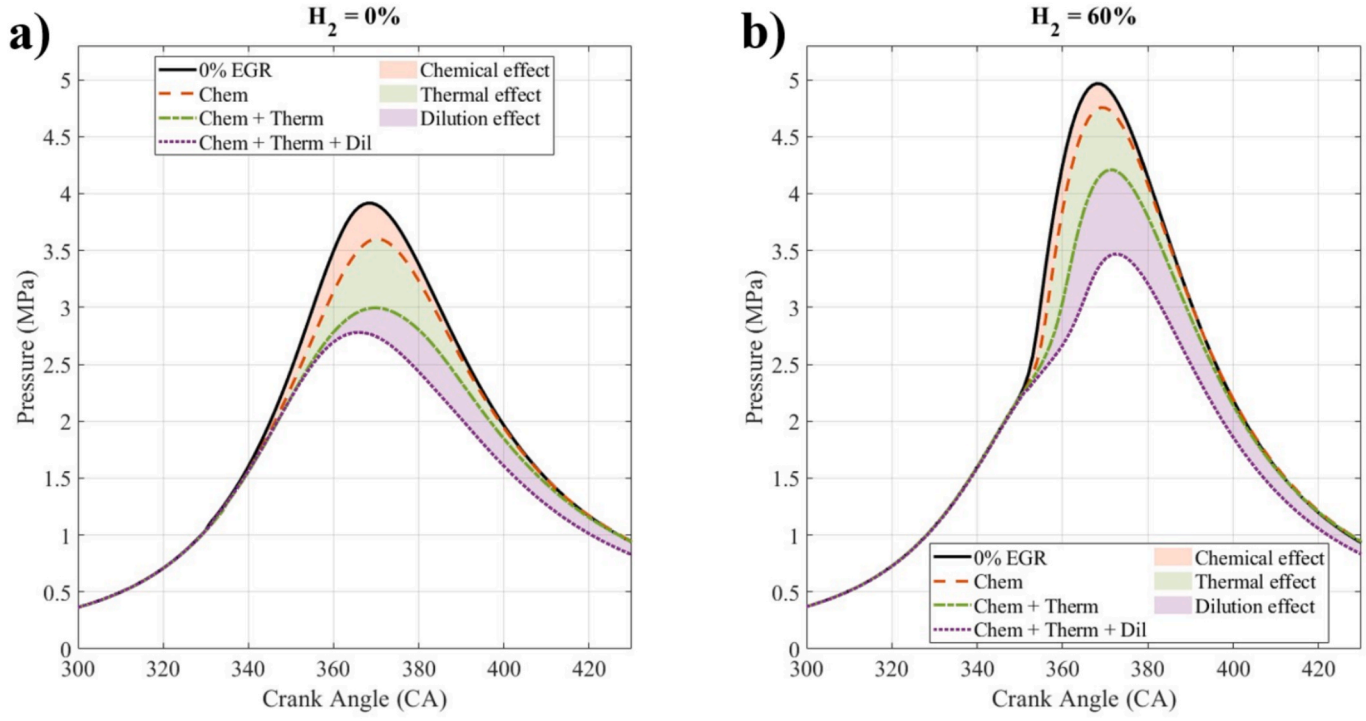

Fig. 10. Isolated effect of the isolated effect of the dilution, thermal and chemical effects of EGR addition on the in-cylinder pressure of a) neat ammonia and b) ammonia with 60% hydrogen addition percentage (λ = 1, MAP = 110 kPa, $ST_{X_{H_2}=0}$=38 °CA bTDC, $ST_{X_{H_2}=0.6}$=13 °CA bTDC).

the combustion chamber, which reduces the effective energy release per unit mass of mixture. Furthermore, it can be seen from Fig. 10 that the thermal and dilution effects were the dominant mechanisms governing the decrease in in-cylinder pressure with EGR addition, primarily due to the increased heat capacity of the mixture and the reduction in reactive mixture amount, respectively.

3.3.2. *Burn rate of ammonia with hydrogen*

Fig. 11a shows the simulated ammonia combustion phasing for various excess air ratios at MBT timing and a manifold air pressure of 110 kPa. The total combustion duration, CA0-90, is defined as the crank angle interval required to burn the bulk of the in-cylinder fuel–air mixture from 0% to 90%. For richer mixtures, the MBT was closer to TDC, meaning combustion occurred at higher pressures and temperatures, which would eventually increase the flame speed, consequently accelerating the combustion. It could be seen from Fig. 11a that as the excess air ratio increases, the total combustion duration increased for leaner ammonia mixtures. Specifically, the total combustion duration increased by 43% when the excess air ratio increased from stoichiometric conditions to an excess air ratio of 1.5. This was caused by the slower flame speed resulting from an increased air dilution, and by the greater flame development angle (CA0-10) and the interval required to burn the bulk of the in-cylinder mixture from 10% to 90% (CA10-90). The inherently slow burning rate of ammonia could be improved by adding hydrogen. The combustion phasing for various hydrogen additions to ammonia at a fixed excess air ratio of 1.2 and a spark timing at MBT timing is shown in Fig. 11b. The addition of hydrogen to the ammonia-fuelled SI engine accelerated both the early flame development phase (CA0-10) and the flame propagation phase (CA10-90), consequently reducing the total combustion duration (CA0-90). This induction lag time was captured through the incorporation of chemical kinetics to determine the LFS, and by linking the LFS with C_τ and $C_{u'}$ through Equations (2) to (6). The total combustion duration of ammonia decreased by 21%, 25%, 40%, and 57% for 10%, 20%, 40%, and 60% hydrogen addition, respectively. This behaviour was primarily because of the enhanced chemical reactivity causing higher LFS of the ammonia with hydrogen enrichment compared to neat ammonia [32]. The combustion phasing of hydrogen enriched ammonia mixtures aligns with the LFS across various hydrogen additions, excess air ratios, and EGR rates, as shown in Figs. 11 and 12. This simulated combustion phasing result agrees with experimental observations of a hydrogen-enriched ammonia SI engine under different spark timings and excess air ratios [10]. The effect of EGR addition on the combustion phasing of hydrogen-enriched ammonia SI engine at excess air ratios of 1 and 1.5 are shown in Fig. 12a and b, respectively. It can be seen that EGR addition slowed down the combustion of the hydrogen enriched ammonia SI engine under all the simulated engine operating conditions. The increase in total combustion duration with EGR addition was due to the reduction in laminar flame speed and the variation in the thermodynamic properties of the diluted mixture under different percentages of EGR addition. The increase in combustion duration with EGR could affect combustion stability; however, this effect could not be resolved by the two-zone combustion model.

3.4. *NO_X emissions and indicated specific fuel consumption*

The crank angle resolved in-cylinder temperature and pressure calculated from the two-zone combustion model were used in Chemkin Pro using the kinetic mechanism of [20] to calculate the instantaneous evolution of the nitric oxide (NO), nitrous oxide (N_2O), and nitrogen dioxide (NO_2). Fig. 13 shows the in-cylinder evolution of NO, N_2O, and NO_2 for different hydrogen addition percentages and EGR of the ammonia-fuelled SI engine under MBT timing. As it could be seen from Fig. 13a the addition of hydrogen to ammonia increases the concentrations of NO and NO_2 species due to the higher combustion temperatures and faster flame propagation in hydrogen-enriched mixtures. The NO has the highest concentration, and its formation increases with hydrogen addition as a result of enhanced NO production through the

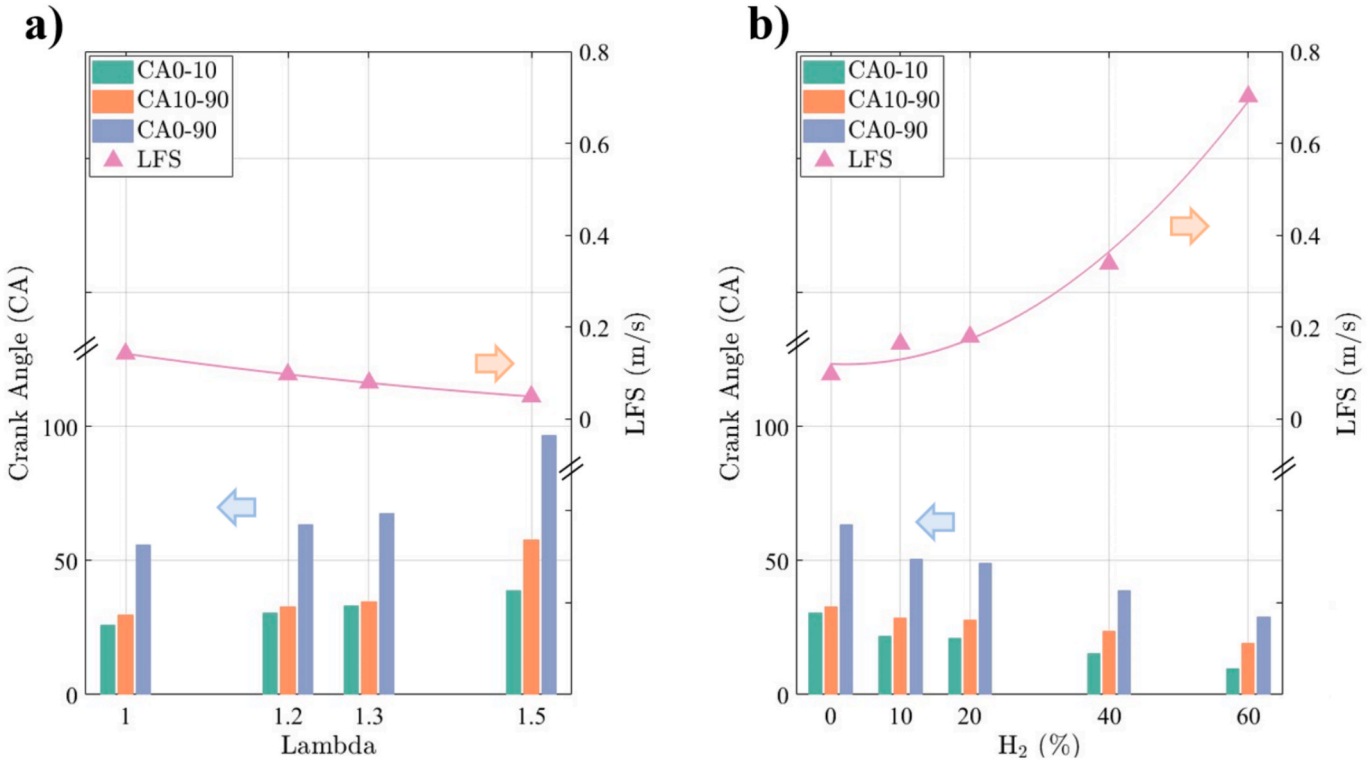

Fig. 11. a) Simulated combustion phasing for neat ammonia under various excess air ratios at MAP = 110 kPa (CR = 10.5, N = 1500 rpm, ST = MBT) and b) simulated ammonia combustion phasing for various percentages of hydrogen enrichment under an excess air ratio of 1.2 at MAP = 110 kPa (CR = 10.5, N = 1500 rpm, ST = MBT).

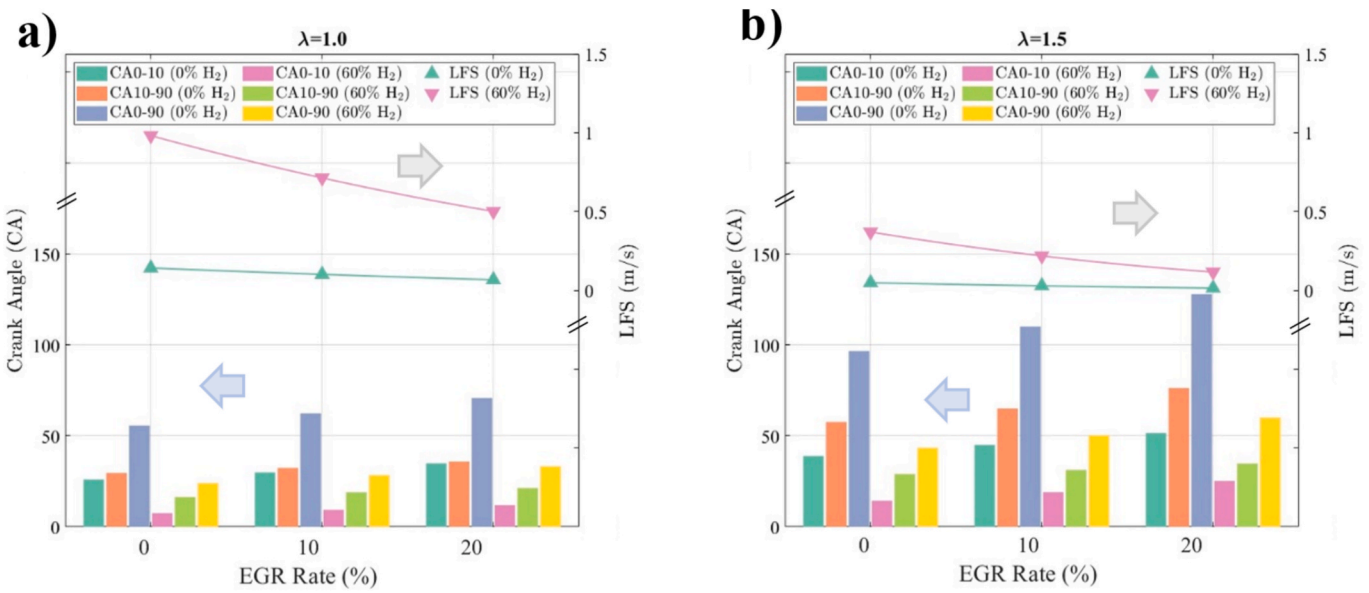

Fig. 12. a) Simulated combustion phasing under excess air ratio of 1 for various hydrogen additions and EGR rates (CR = 10.5, N = 1500 rpm, ST = MBT) and b) simulated combustion phasing under excess air ratio of 1.5 for various hydrogen additions and EGR rates (CR = 10.5, N = 1500 rpm, ST = MBT).

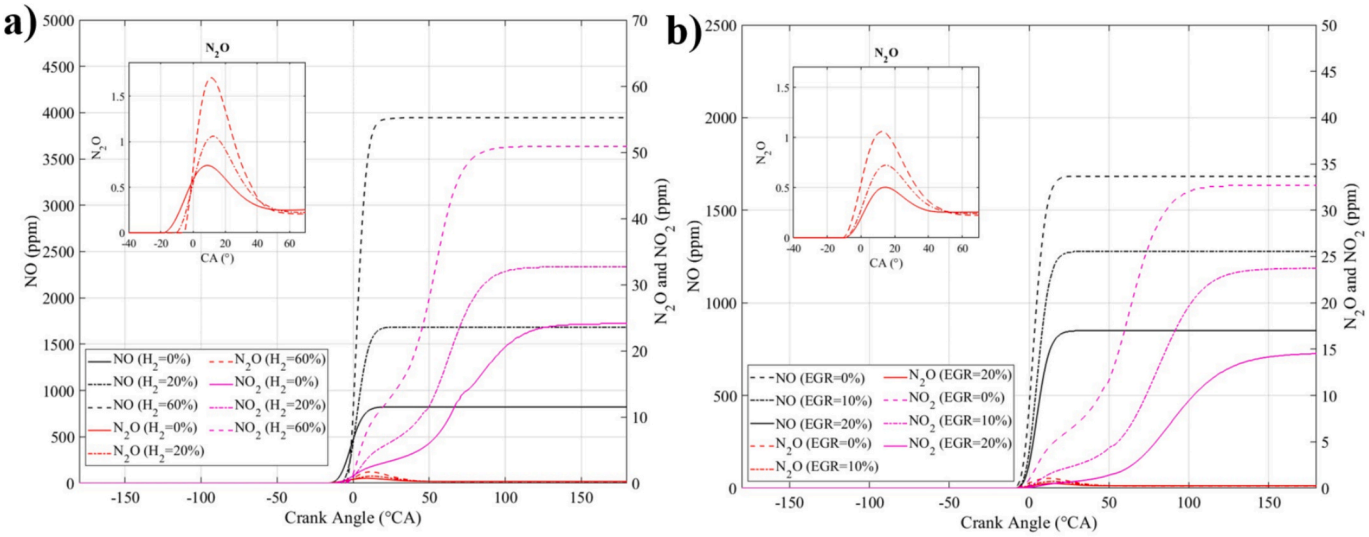

Fig. 13. NO, N_2O, and NO_2 emissions for a) ammonia with different hydrogen addition percentages, and b) ammonia with 20% hydrogen addition at various EGR rates (λ = 1.2, MAP = 110 kPa).

reaction N_2 + O=NO + N, described by the Zeldovich mechanism. Moreover, it can be seen that the N_2O concentration rises during combustion and then decreases to a constant value as N_2O molecules are consumed, which agrees with the heat release behaviour of ammonia combustion [35]. N_2O is mainly produced through the reaction NH + NO=N_2O + H [36]. But it can be seen from Fig. 13b that the N_2O increased with the addition of EGR to ammonia SI engine, due to the decrease of the in-cylinder temperature with EGR addition which limited the consumption of N_2O. Moreover, the EGR was effective on the reduction of the NO and NO_2 due to the combined thermal and dilution effects, which lower in-cylinder temperatures [16]. Fig. 14 shows that increasing EGR rate reduces NO emissions but simultaneously increases ISFC at a given percentage of hydrogen enrichment. This was due to the decrease of the thermal efficiency due to the lower combustion temperatures and reduced flame speeds associated with EGR dilution. For ammonia with 20% hydrogen addition percentage under an excess air ratio of 1.2, NO emissions were reduced by 48%, while ISFC increased by 10% for 20% EGR addition. But in reality, the emissions would be higher due to unburned ammonia, especially under highly diluted mixture conditions, which were not captured in this study [37].

4. Conclusions

A two-zone combustion model with a detailed chemistry to calculate the laminar flame speed for hydrogen enriched ammonia combustion and the mass fraction burn rate was developed to incorporate C_τ and $C_{u'}$ to account for flow and reaction to predict the performance of a hydrogen-enriched ammonia SI engine. It was observed that the standard entrainment based two-zone combustion model could not accurately predict the early flame development angle compared to experimental data. This limitation was mainly due to the very low flame speed of ammonia mixtures, making the flame more sensitive to instabilities. Nevertheless, the developed mass fraction burn model was able to predict the performance of the ammonia hydrogen SI engine

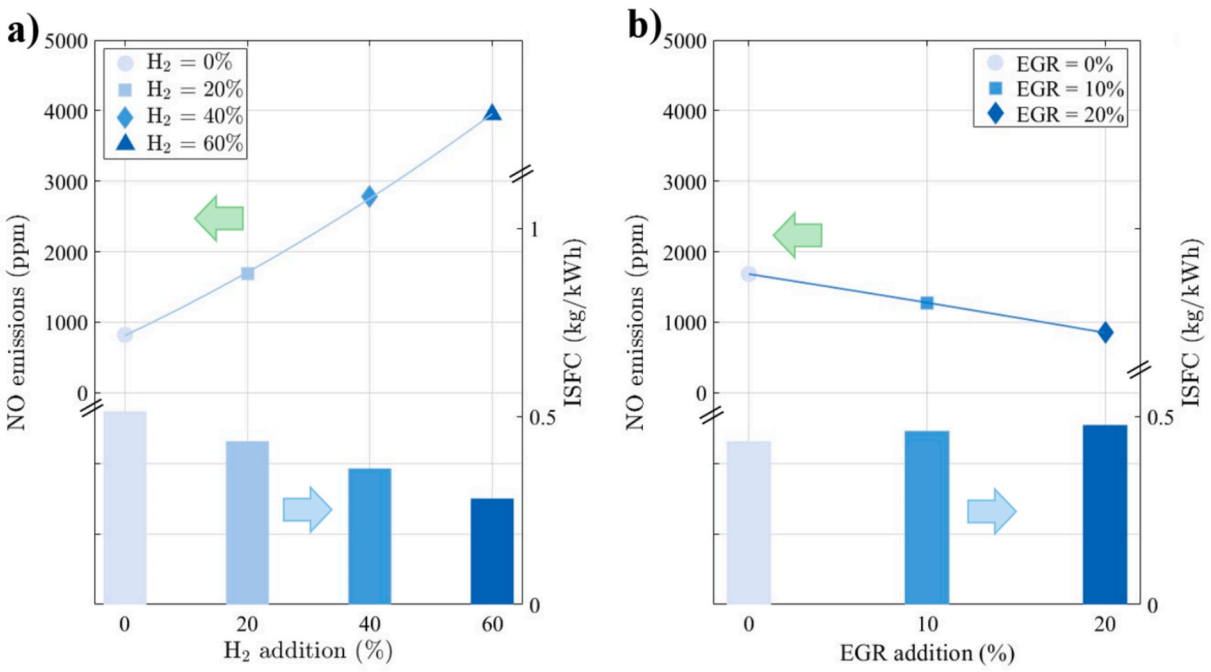

Fig. 14. a) NO emissions and indicated specific fuel consumption of ammonia with different hydrogen addition percentages (λ = 1.2, MAP = 110 kPa), and b) NO emissions and indicated specific fuel consumption at different EGR rates of ammonia with 20% hydrogen addition percentage (λ = 1.2, MAP = 110 kPa).

when compared to experimental results with an accuracy of within 5%. The predicted combustion phasing of hydrogen enriched ammonia was then used in a two-zone combustion model to estimate the performance of the hydrogen-ammonia SI engine under various operating conditions, including EGR. The two-zone combustion model showed good agreement with experimental in-cylinder pressure data with standard error less than 4%. Simulations showed that hydrogen addition shortened the combustion duration of the ammonia SI engine across all excess air ratios. This was primarily due to the enhanced chemical reactivity and higher laminar flame speeds of the ammonia-hydrogen mixtures compared to neat ammonia. For a given excess air ratio, hydrogen enrichment improved the IMEP at all addition percentages compared to neat ammonia operation. For all excess air ratios, the highest IMEP occurred at 10% hydrogen addition. The IMEP decreased for hydrogen additions above 10%, which was attributed to just sufficient energy input due to the high stoichiometric air–fuel ratio of hydrogen compared to neat ammonia. The developed two-zone model is capable of capturing the EGR effect through flame speed reduction and the variation of thermodynamic properties of hydrogen-enriched ammonia mixtures, also explains the observed decline in IMEP with increasing EGR rates. For ammonia with 20% hydrogen addition percentage under an excess air ratio of 1.2 the NO emissions decreased by 48% and ISFC increased by 10% for 20% EGR addition.

CRediT authorship contribution statement

D.N. Rrustemi: Writing – original draft, Visualization, Methodology. **T. Megaritis:** Writing – review & editing, Supervision, Methodology. **L.C. Ganippa:** Writing – review & editing, Supervision, Methodology, Investigation.

Declaration of competing interest

The authors declare that they have no known competing financial interests or personal relationships that could have appeared to influence the work reported in this paper.

Acknowledgements

We acknowledge the financial support of Engineering and Physical Sciences Research Council (EPSRC) of the UK under Grant No. EP/X019578/1.

Appendix

A.1. Exhaust gas recirculation composition

The Fig. A1 shows the EGR chemical composition at different hydrogen addition percentage maintained at various excess air ratios.

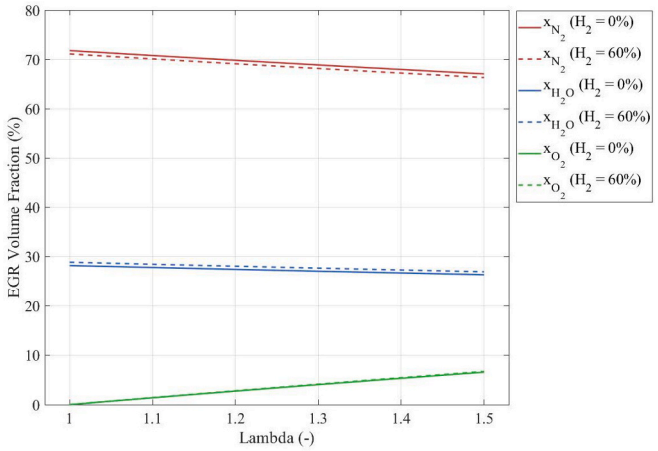

Fig. A1. Exhaust species volume fractions at various excess air ratio with different hydrogen addition percentage.

A.2. Correcting constants fitting

The linear regression for C_τ and $C_{u'}$ is given as:

$$C_\tau = a_0 + a_1 L_T + a_2 S_L$$

$$C_{u'} = b_0 + b_1 u' + b_2 S_L$$

In Fig. A2, the x-axis shows the correction constants C_τ and $C_{u'}$ extracted from experimental combustion phasing, while the y-axis shows the corresponding values predicted by linear regression. C_τ, fitted using the Taylor microscale and laminar flame speed, showed a strong correlation (R^2 = 0.978), indicating its strong dependence on flame speed. In contrast, $C_{u'}$ fitted using turbulence intensity and laminar flame speed, showed no clear correlation (R^2 = 0.615).

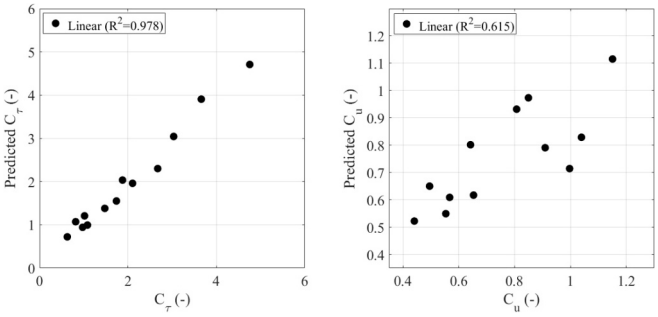

Fig. A2. Extracted values of a) and b) compared to the simulated values of these coefficients using linear regression (CR = 10.5, MAP = 120 kPa, N = 1500 rpm).

A.3. Two-zone combustion model

After rearranging the equation of state, the first law and continuity equation, following first order differential equations were derived to model combustion process. The subscript u and b refer to unburned and burned zone, respectively [38].

$$\frac{dT_u}{d\theta} = \frac{1}{m_u c_{pu}}\left(V_u \frac{dP}{d\theta} + \frac{dQ_u}{d\theta}\right)$$

$$\frac{dT_b}{d\theta} = \frac{1}{m_u c_{pu}}\left[P\frac{dV}{d\theta} - (R_b T_b - R_u T_u)\frac{dm_b}{d\theta} - \frac{R_u}{c_{pu}}\left(V_u \frac{dP}{d\theta} + \frac{dQ_u}{d\theta}\right) + V\frac{dP}{d\theta}\right]$$

$$\frac{dP}{d\theta} = \frac{1}{\frac{c_{vu}}{c_{pu}}V_u - \frac{c_{vb}R_u}{R_b c_{pu}}V_u + \frac{c_{vb}}{R_b}V}\left\{\left(1 + \frac{c_{vb}}{R_b}\right)P\frac{dV}{d\theta} - \frac{dQ}{d\theta} + \left[(u_b - u_u) - c_{vb}\left(T_b - \frac{R_u}{R_b}T_u\right)\right]\frac{dm_b}{d\theta} + \left(\frac{c_{vu}}{c_{vb}} - \frac{c_{vb}R_u}{R_b c_{pu}}\right)\frac{dQ_u}{d\theta}\right\}$$

where T_b and T_u are the temperatures of the burned and unburned zones, respectively. m_b and m_u are the masses of the burned and unburned gases, and c_{pu} is specific heat at constant pressure of the unburned zone. θ is the crank angle. c_{vb} and c_{vu} are the specific heat capacities at constant volume of the burned and unburned gases, respectively. V_u is the volume of the unburned zone, V is the volume of the chamber, and P is the in-cylinder pressure. R_b and R_u are the gas constants of the burned and unburned gases, respectively. $\frac{dQ}{d\theta}$ is the gross convective heat transfer rate and $\frac{dQ_u}{d\theta}$ represent the rates

of heat transfer in the unburned zone heat transfer. u_b and u_u are internal energy of the burned and unburned zones, respectively.

The gross convective heat transfer was calculated as;

$$\frac{dQ}{d\theta} = \frac{dQ_u}{d\theta} + \frac{dQ_b}{d\theta}$$

The convective heat transfer was modelled based on Woschni approach [39].

The thermodynamic properties of hydrogen enriched ammonia mixture at various operating conditions were calculated using the NASA polynomial [40]. The specific heat, and standard state enthalpy were calculated as;

$$\frac{c_p(T)}{\widetilde{R}} = a_1 + a_2T + a_3T^2 + a_4T^3 + a_5T^4$$

$$\frac{h(T)}{\widetilde{R}} = a_1 + \frac{a_2T}{2} + \frac{a_3T^2}{3} + \frac{a_4T^3}{4} + \frac{a_5T^4}{5} + \frac{a_6}{T}$$

The values for the coefficient a_i for are taken from [40].

Data availability

Data will be made available on request.

References

[1] Chehade G, Dincer I. Progress in green ammonia production as potential carbon-free fuel. Fuel 2021;299:120845. https://doi.org/10.1016/j.fuel.2021.120845.

[2] Manigandan S, Ryu JI, Praveen Kumar TR, Elgendi M. Hydrogen and ammonia as a primary fuel – a critical review of production technologies, diesel engine applications, and challenges. Fuel 2023;352:129100. https://doi.org/10.1016/j.fuel.2023.129100.

[3] Yan Z, Peters N, Harrington A, Bunce M, Hall J. Investigation of ammonia-fueled SI combustion in a high tumble engine, Detroit, Michigan. United States 2024, 2024–01–2815.. https://doi.org/10.4271/2024-01-2815.

[4] Frigo S, Gentili R. Analysis of the behaviour of a 4-stroke Si engine fuelled with ammonia and hydrogen. Int J Hydrog Energy 2013;38:1607–15. https://doi.org/10.1016/j.ijhydene.2012.10.114.

[5] Yan Y, Liu Z, Liu J. An Evaluation of the conversion of gasoline and natural gas spark ignition engines to ammonia/hydrogen operation from the perspective of laminar flame speed. J Energy Res Technol 2023;145:012302. https://doi.org/10.1115/1.4054754.

[6] Boretti A. Hydrogen internal combustion engines to 2030. Int J Hydrog Energy 2020;45:23692–703. https://doi.org/10.1016/j.ijhydene.2020.06.022.

[7] Rrustemi DN, Ganippa LC, Megaritis T, Axon CJ. New laminar flame speed correlation for lean mixtures of hydrogen combustion with water addition under high pressure conditions. Int J Hydrog Energy 2024;63:609–17. https://doi.org/10.1016/j.ijhydene.2024.03.177.

[8] Mørch CS, Bjerre A, Gøttrup MP, Sorenson SC, Schramm J. Ammonia/hydrogen mixtures in an SI-engine: engine performance and analysis of a proposed fuel system. Fuel 2011;90:854–64. https://doi.org/10.1016/j.fuel.2010.09.042.

[9] Li J, Zhang R, Pan J, Wei H, Shu G, Chen L. Ammonia and hydrogen blending effects on combustion stabilities in optical SI engines. Energy Convers Manag 2023;280:116827. https://doi.org/10.1016/j.enconman.2023.116827.

[10] Lhuillier C, Brequigny P, Contino F, Mounaïm-Rousselle C. Experimental study on ammonia/hydrogen/air combustion in spark ignition engine conditions. Fuel 2020;269:117448. https://doi.org/10.1016/j.fuel.2020.117448.

[11] Dinesh MH, Pandey JK, Kumar GN. Study of performance, combustion, and NOx emission behavior of an SI engine fuelled with ammonia/hydrogen blends at various compression ratio. Int J Hydrog Energy 2022;47:25391–403. https://doi.org/10.1016/j.ijhydene.2022.05.287.

[12] Novella R, Pastor J, Gomez-Soriano J, Sánchez-Bayona J. Numerical study on the use of ammonia/hydrogen fuel blends for automotive spark-ignition engines. Fuel 2023;351:128945. https://doi.org/10.1016/j.fuel.2023.128945.

[13] Voniati G, Dimaratos A, Koltsakis G, Ntziachristos L. Ammonia as a marine fuel towards decarbonization: emission control challenges. Sustainability 2023;15:15565. https://doi.org/10.3390/su152115565.

[14] Yang R, Liu Z, Liu J. The methodology of decoupling fuel and thermal nitrogen oxides in multi-dimensional computational fluid dynamics combustion simulation of ammonia-hydrogen spark ignition engines. Int J Hydrog Energy 2024;55:300–18. https://doi.org/10.1016/j.ijhydene.2023.09.105.

[15] Song B, Lin R, Lam CH, Wu H, Tsui T-H, Yu Y. Recent advances and challenges of inter-disciplinary biomass valorization by integrating hydrothermal and biological techniques. Renew Sustain Energy Rev 2021;135:110370. https://doi.org/10.1016/j.rser.2020.110370.

[16] Masoumi S, Houshfar E, Ashjaee M. Experimental and numerical analysis of ammonia/hydrogen combustion under artificial exhaust gas recirculation. Fuel 2024;357:130081. https://doi.org/10.1016/j.fuel.2023.130081.

[17] Lee S, Park C, Park S, Kim C. Comparison of the effects of EGR and lean burn on an SI engine fueled by hydrogen-enriched low calorific gas. Int J Hydrog Energy 2014;39:1086–95. https://doi.org/10.1016/j.ijhydene.2013.10.144.

[18] Al-Qurashi K, Lueking AD, Boehman AL. The deconvolution of the thermal, dilution, and chemical effects of exhaust gas recirculation (EGR) on the reactivity of engine and flame soot. Combust Flame 2011;158:1696–704. https://doi.org/10.1016/j.combustflame.2011.02.006.

[19] Zitouni S, Brequigny P, Mounaïm-Rousselle C. Turbulent flame speed and morphology of pure ammonia flames and blends with methane or hydrogen. Proc Combust Inst 2023;39:2269–78. https://doi.org/10.1016/j.proci.2022.07.179.

[20] Zhu Y, Curran HJ, Girhe S, Murakami Y, Pitsch H, Senecal K, et al. The combustion chemistry of ammonia and ammonia/hydrogen mixtures: a comprehensive chemical kinetic modeling study. Combust Flame 2024;260:113239. https://doi.org/10.1016/j.combustflame.2023.113239.

[21] Girhe S, Snackers A, Lehmann T, Langer R, Loffredo F, Glaznev R, et al. Ammonia and ammonia/hydrogen combustion: comprehensive quantitative assessment of kinetic models and examination of critical parameters. Combust Flame 2024;267:113560. https://doi.org/10.1016/j.combustflame.2024.113560.

[22] Liu K, Burluka AA, Sheppard CGW. Turbulent flame and mass burning rate in a spark ignition engine. Fuel 2013;107:202–8. https://doi.org/10.1016/j.fuel.2013.01.042.

[23] Yıldız M, Albayrak ÇB. Zero-dimensional single zone engine modeling of an SI engine fuelled with methane and methane-hydrogen blend using single and double Wiebe Function: a comparative study. Int J Hydrog Energy 2017;42:25756–65. https://doi.org/10.1016/j.ijhydene.2017.07.016.

[24] Kuppa K, Nguyen HD, Goldmann A, Korb B, Wachtmeister G, Dinkelacker F. Numerical modelling of unburned hydrocarbon emissions in gas engines with varied fuels. Fuel 2019;254:115532. https://doi.org/10.1016/j.fuel.2019.05.115.

[25] Nguyen D-K, Sileghem L, Verhelst S. A quasi-dimensional combustion model for spark ignition engines fueled with gasoline–methanol blends. Proc Inst Mech Eng Part J Automob Eng 2018;232:57–74. https://doi.org/10.1177/0954407017728161.

[26] Ji C, Yang J, Liu X, Zhang B, Wang S, Gao B. A quasi-dimensional model for combustion performance prediction of an SI hydrogen-enriched methanol engine. Int J Hydrog Energy 2016;41:17676–86. https://doi.org/10.1016/j.ijhydene.2016.07.146.

[27] Ma F, Li S, Zhao J, Qi Z, Deng J, Naeve N, et al. A fractal-based quasi-dimensional combustion model for SI engines fuelled by hydrogen enriched compressed natural gas. Int J Hydrog Energy 2012;37:9892–901. https://doi.org/10.1016/j.ijhydene.2012.03.045.

[28] Shrestha KP, Lhuillier C, Barbosa AA, Brequigny P, Contino F, Mounaïm-Rousselle C, et al. An experimental and modeling study of ammonia with enriched oxygen content and ammonia/hydrogen laminar flame speed at elevated pressure and temperature. Proc Combust Inst 2021;38:2163–74. https://doi.org/10.1016/j.proci.2020.06.197.

[29] Ma F, Liu H, Wang Y, Wang J, Ding S, Zhao S. A quasi-dimensional combustion model for SI engines fuelled by hydrogen enriched compressed natural gas, 2008, 2008-01-1633. 10.4271/2008-01-1633.

[30] Conte E, Boulouchos K. A Quasi-Dimensional Model for Estimating the Influence of Hydrogen-Rich Gas Addition on Turbulent Flame Speed and Flame Front Propagation in IC-SI Engines, 2005, 2005-01-0232. 10.4271/2005-01-0232.

[31] Krebs S, Biet C. Predictive model of a premixed, lean hydrogen combustion for internal combustion engines. Transp Eng 2021;5:100086. https://doi.org/10.1016/j.treng.2021.100086.

[32] Figueroa-Labastida M, Zheng L, Streicher JW, Hanson RK. Ammonia/hydrogen laminar flame speed measurements at elevated temperatures. Int J Hydrog Energy 2024;63:1137–46. https://doi.org/10.1016/j.ijhydene.2024.03.255.

[33] Liang W, Law CK. Enhancing ammonia combustion using reactivity stratification with hydrogen addition. Proc Combust Inst 2023;39:4419–26. https://doi.org/10.1016/j.proci.2022.10.025.

[34] Duan X, Li Y, Liu Y, Zhang S, Guan J, Lai M-C, et al. Dilution gas and hydrogen enrichment on the laminar flame speed and flame structure of the methane/air mixture. Fuel 2020;281:118794. https://doi.org/10.1016/j.fuel.2020.118794.

[35] Bjørgen KOP, Emberson DR, Løvås T. Combustion of liquid ammonia and diesel in a compression ignition engine operated in high-pressure dual fuel mode. Fuel 2024;360:130269. https://doi.org/10.1016/j.fuel.2023.130269.

[36] Glarborg P, The NH. 3 /NO 2 /O 2 system: constraining key steps in ammonia ignition and N 2 O formation. Combust Flame 2023;257:112311. https://doi.org/10.1016/j.combustflame.2022.112311.
[37] Cova-Bonillo A, Gabana P, Khedkar N, Brinklow G, Wu M, Herreros JM, et al. Predicting NOx emissions from ammonia engines – fuel and thermal effects. Int J Hydrog Energy 2025;187:150734. https://doi.org/10.1016/j.ijhydene.2025.150734.
[38] Rrustemi DN, Ganippa LC, Megaritis T, Axon CJ. Predicting hydrogen engine performance with water addition using a two-zone thermodynamic model. Fuel 2025;386:134137. https://doi.org/10.1016/j.fuel.2024.134137.
[39] Woschni G. A Universally Applicable Equation for the Instantaneous Heat Transfer Coefficient in the Internal Combustion Engine, 1967, 670931. 10.4271/670931.
[40] Heywood JB. Internal combustion engine fundamentals. New York: Mcgraw-Hill Education; 2018.